Journal of Power Sources 196 (2011) 9528–9535

Contents lists available at ScienceDirect

Journal of Power Sources

journal homepage: www.elsevier.com/locate/jpowsour

Preparation of functional layers for anode-supported solid oxide fuel cells by the reverse roll coating process

R. Mücke[a,*], O. Büchler[a], M. Bram[a], A. Leonide[b], E. Ivers-Tiffée[b,c], H.P. Buchkremer[a]

[a] Forschungszentrum Jülich, Institute of Energy and Climate Research (IEK-1), D-52425 Jülich, Germany
[b] Institute of Materials for Electrical Engineering (IWE), Karlsruhe Institute of Technology (KIT), D-76131 Karlsruhe, Germany
[c] DFG Center for Functional Nanostructures (CFN), Karlsruhe Institute of Technology (KIT), D-76131 Karlsruhe, Germany

ARTICLE INFO

Article history:
Received 11 April 2011
Received in revised form 23 June 2011
Accepted 18 July 2011
Available online 22 July 2011

Keywords:
Reverse roll coating
Industrial coating process
Single step co-firing of half-cells
Solid oxide fuel cell
Electrochemical impedance spectra

ABSTRACT

The roll coating technique represents a novel method for applying functional layers to solid oxide fuel cells (SOFCs). This fast process is already used for mass production in other branches of industry and offers a high degree of automation. It was utilized for coating specially developed anode (NiO + 8YSZ, 8YSZ: 8 mol% yttria-stabilized zirconia) and electrolyte (8YSZ) suspensions on green and pre-sintered tape-cast anode supports (NiO + 8YSZ). The layers formed were co-fired in a single step at 1400 °C for 5 h. As a result, the electrolyte exhibited a thickness of 14–18 μm and sufficient gas tightness. Complete cells with a screen-printed and sintered $La_{0.65}Sr_{0.3}MnO_{3-\delta}$ (LSM)/8YSZ cathode yielded a current density of 0.9–1.1 A cm^{-2} at 800 °C and 0.7 V, which is lower than the performance of non-co-fired slip-cast or screen-printed Jülich standard cells with thinner anode and electrolyte layers. The contribution of the cell components to the total area-specific resistance (ASR) was calculated by analyzing the distribution function of the relaxation times (DRTs) of measured electrochemical impedance spectra (EIS) and indicates the potential improvement in the cell performance achievable by reducing the thickness of the roll-coated layers. The results show that the anode-supported planar half-cells can be fabricated cost-effectively by combining roll coating with subsequent co-firing.

1. Introduction

Significant advances have been reported for increasing the performance of planar SOFCs and their durability by employing new materials with an optimized microstructure and modern coating technologies [1–6]. Recent examples include plasma-sprayed protective coatings on the interconnects, which allowed degradation rates as low as 3 mV/1000 h [5], and thin-film electrolytes with a thickness of 1.0–1.5 μm applied by sol–gel technology yielding the highest performance of SOFCs to date [6]. In addition, high-throughput manufacturing processes that allow low manufacturing costs are required to bring the SOFC technology to market. Among all SOFC cell designs, planar anode-supported cells yield the highest power output. They are therefore mainly used to build stacks with high power densities, e.g. for mobile and smaller stationary applications. Tape casting is considered a viable industrial manufacturing process for anode and electrolyte substrates and is already widely used [1,7]. The functional layers are commonly applied by screen printing [8–10] or wet powder spraying [2,11]. Whereas wet powder spraying suffers from a relatively large overspray, and spraying hazardous materials like NiO represents a safety issue, screen printing is a batch processes and therefore limited in speed. Interesting alternatives to both methods are to laminate tape-cast functional layers on a support in its green state [12] or to directly tape cast complete half-cells starting with the electrolyte (reverse tape-cast cell [7]). With these methods, it is possible to apply thin coatings with a thickness of a few micrometers on green tapes over their total length before the multi-layer system is decollated and co-fired.

Roll coating represents a scalable and very simple coating technique. It allows continuous coating on either sintered or green substrates; even contoured coatings are feasible with appropriate rolls (gravure coating [13] or relief printing). Defect-free wet coatings of 12–1200 μm thickness can be applied with industrial machines at speeds of approx. 1–500 m min^{-1}, utilizing coating liquids with a large range of viscosities (0.05–500 Pa s) [14]. With sol–gels as coating liquids, dried thicknesses as low as 1 μm were reported [15], thus demonstrating the feasibility of coating thin films by reverse roll coating. Whereas the roll coating process is widely used in the paper, textile, metal, optical and electronic industry, and also in the manufacturing of PEM fuel cells [16], it has yet not been applied to SOFC manufacturing.

* Corresponding author. Tel.: +49 2461 614066; fax: +49 2461 612455.
E-mail address: r.muecke@fz-juelich.de (R. Mücke).

0378-7753/$ – see front matter © 2011 Elsevier B.V. All rights reserved.
doi:10.1016/j.jpowsour.2011.07.063

Table 1
Materials and composition of the anode and electrolyte suspension used.

	Solid content	Solvent	Binder
Anode	22.4 wt.% NiO (J.T. Baker)17.6 wt.% 8YSZ (TZ-8Y)	58 wt.% dibasic esters	2 wt.% ethyl cellulose 45–55 mPa s
Electrolyte	40 wt.% 8YSZ (TZ-8Y)	58 wt.% dibasic esters	2 wt.% ethyl cellulose 45–55 mPa s

Depending on the orientation of rotation of the applicator roll relative to the sample being coated, two varieties of the roll coating process can be distinguished: forward and reverse roll coating. During reverse roll coating, the applicator roll rotates opposite to the transport direction of the sample. This coating method, which was first described by Münch [17], can achieve an even distribution of the coated liquid on irregular surfaces [18] and is known to display less surface instabilities, such as ribbing phenomena, than forward roll coating, especially if non-Newtonian liquids are processed [19,20]. Recognizing these advantages, the layers in this work were applied using reverse roll coating. Both green tapes and pre-sintered anode supports were coated with an anode and electrolyte layer prepared from submicron powders utilizing an advanced, commercially available laboratory reverse roll coater with a maximum transport speed of 60 m min^{-1}. In this work, transport speeds of 5 m min^{-1} were used, which is already much higher than the coating speeds of any other coating process Jülich has utilized in the past.

Advanced analysis of the electrochemical impedance spectra allowed us to correlate the observed microstructural properties of the manufactured cells, e.g. the layer thickness, with the electrochemical performance [21]. Utilizing the distribution function of relaxation times (DRTs), the ASR of single cell components could be calculated and used for the interpretation of the obtained data.

2. Experimental

2.1. Substrates

The porous ceramic substrates were prepared by tape casting starting from commercially available 8YSZ powder (FYT13.0-005H, Unitec Ceramics Ltd., Stafford, U.K.) and NiO powder (Mallinckrodt Baker Inc., Phillipsburg, NJ). The tape casting slurry was based on a solvent mixture of ethanol/methyl ethyl ketone. Additionally, it contained a dispersant (Nuosperse FX9086, Elementis Specialities Inc., Hightstown, NJ), a binder (polyvinyl butyral) and plasticizers (polyethylene glycol/Solusolv S-2075, Solutia Deutschland GmbH, Frankfurt, Germany). First, 60 wt.% NiO and 40 wt.% 8YSZ powder were homogenized with the dispersant in the solvent. Further organic additives, such as the binder and plasticizer, were then added in an adequate ratio to produce a slurry with well-adapted rheological properties [7,23]. Then, the slip was degassed. Due to lack of availability of this newly developed slip, some coatings were applied on a tape produced with a slightly different recipe described in Ref. [24]. For this recipe partly different organics and a graphite pore former was used. Both tapes displayed the same performance during electrochemical quality assurance tests (as the cell performance is governed by the functional layers) and can be, in this respect, considered interchangeable. All tapes were cast by the well-known doctor blade process (FGA 500, SAMA Maschinenbau GmbH, Weißenstadt, Germany) and subsequently dried. Finally, the green substrate tapes with a thickness of 0.58 mm were cut into dimensions of 200 mm × 120 mm. Some tapes, prepared from the recipe described in Ref. [23], were used in the green state as coating supports. Other tapes, prepared from the recipe according to Ref. [24], were debindered and pre-sintered at 1230 °C for 3 h, thereby shrinking to dimensions of approx. 184 mm × 110 mm × 0.53 mm. This cell format was chosen because such cells can be used in lightweight stacks in future work [25].

2.2. Coating and sintering

The ceramic starting material for the production of the anode layer was a mixture composed of 56 wt.% NiO (Mallinckrodt Baker Inc., Phillipsburg, NJ) and 44 wt.% 8YSZ (TZ-8Y, Tosoh Corp., Tokyo, Japan). Before mixing the two powders in ethanol, the NiO was ground in ethanol to an average grain size of about 0.3 μm. The 8YSZ powder was calcined at 1230 °C for 3 h and then wet ball-milled to 0.5 μm. The calcined 8YSZ was used for the anode and electrolyte layer. The roll coating suspensions for both layers were prepared in the same way. A mixture of succinic, glutaric and adipic acid dimethyl esters, also known as dibasic ester (DBE), was chosen as the solvent (INVISTA Resins & Fibers GmbH, Hattersheim am Main, Germany). Low vapor pressure, low price and good environmental compatibility render DBE a suitable organic solvent for industrial applications. Another important fact is that it does not react with the rubber coating of the applicator roll. The solvent was mixed with an ethyl cellulose binder to prevent drying cracks in the coatings and to reach a promising green density and strength. The dry ceramic powders were added to the binder solution, and then homogenized with 10 mm zirconia grinding balls for 170 h on a roller bench to achieve an agglomerate-free suspension. The detailed composition of the anode and electrolyte suspension is summarized in Table 1. The lick roll always remained in contact with the applicator roll and rotated in the same orientation and at the same speed as the transport roll to ensure a constant thickness of the wet film on the applicator roll regardless of the presence of a substrate. Green tapes as well as pre-sintered tapes were directly coated with an anode functional layer by roll coating. After drying for 2 h in a dust-free hood, the electrolyte layer was applied in the same way. All coatings were performed with a laboratory reverse roll coater type RRC-BW 350 from Mathis AG (Oberhasli, Switzerland, Fig. 1a). The functional layers were either applied to the air side or the foil side of the tape to see whether this has any influence on the properties of the functional layers or bending of the cells after sintering.

Fig. 1(b) illustrates the roll coating process. The dip roll rotates in a liquor trough filled with the suspension. Then the suspension is transferred from the dip roll to the rubber-coated applicator roll. The distance between these two rolls influences the coating thickness, and can be precisely set with two precision clock gauges. The speed of both rolls is variable and can be adjusted by two digital displays. From the applicator roll, the suspension is directly applied to the substrate. The substrate is moved under the applicator roll by the rubber-coated transport roll, enabling homogeneous coating of the whole sample surface. The speed of the transport roll is also infinitely variable. The distance between the applicator roll and transport roll can be set according to the substrate thickness. The rotational direction of the transport roll can be chosen in the same or in the opposite direction relative to the applicator roll. Here, all coatings were applied in the reverse mode. Table 2 summarizes the coating parameters used in this study. The different thicknesses of green tapes and pre-sintered substrates resulted in slightly different gap settings. All tests were carried out using cells with a roll-coated anode and electrolyte layer and compared with traditional screen-printed layers. In order interpret the electrochemical impedance spectroscopy data better, cells with a roll-coated electrolyte and no anode layer were also prepared and tested.

Table 2
Coating parameters used for roll coating the anode and electrolyte layers, resulting layer thickness and He leak rates.

Substrate thickness (mm)	Transport roll Speed[b] (m min^{-1})	⇔ Gap size (mm)	Applicator roll Speed[b] (m min^{-1})	⇔ Gap size (mm)	Dip roll Speed[b] (m min^{-1})	Anode Thickness (μm)	Electrolyte Thickness (μm)	Leak rate[a] (hPa dm^3 s^{-1} cm^{-2})
0.58 (green tape)	+5.2	0.38	+10.1	0.035	−4.2	11–13	17–18	2.9×10^{-6}
0.52 (pre-sintered)	+5.2	0.40	+10.1	0.035	−4.2	8–10	14–16	7.8×10^{-7}
0.52 (pre-sintered)[c]	+5.2	0.40	+10.1	0.035	−4.2	Without	14–16	4.1×10^{-6}

[a] He leak rates after sintering in the oxidized state, average of three similar cells.
[b] Positive roll speeds mean clockwise direction, negative speeds counterclockwise.
[c] The cell without an anode was prepared to provide additional information during the EIS characterization.

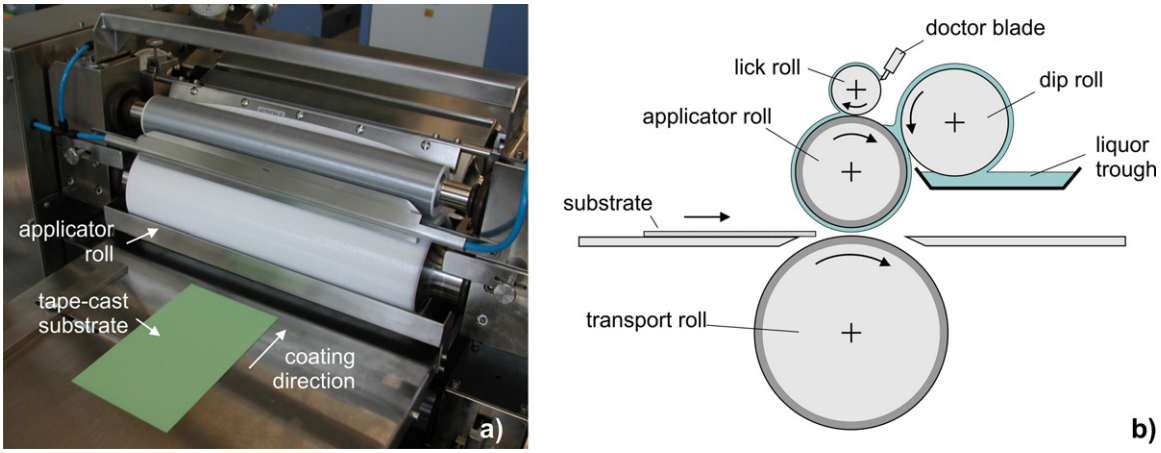

Fig. 1. (a) Schematic of the roll coating process. (b) Reverse roll coater type "RRC-BW" from Mathis AG. A pre-sintered substrate is shown before electrolyte coating.

After drying the roll-coated samples for 2 h at 40 °C in a dust-free hood, the half-cells were sintered at 1400 °C for 5 h. Afterwards, some of them were cut into dimensions of 50 mm × 50 mm for electrochemical characterization and a conventional double-layered cathode was applied by screen printing with the lateral dimensions of 40 mm × 40 mm and 10 mm × 10 mm. The cathode consisted of a $La_{0.65}Sr_{0.3}MnO_{3-\delta}$ (LSM)/8YSZ functional layer with a thickness of approx. 15 μm and an LSM current collector with a thickness of approx. 50 μm and was sintered at 1100 °C for 3 h. The Jülich standard cells were prepared from a pre-sintered substrate (1230 °C for 3 h) and a screen-printed anode and electrolyte, each with a thickness of approx. 7 μm. This anode was calcined after printing at 1000 °C for 1 h before the electrolyte was printed. The other parameters were identical to the cells with roll-coated anodes and electrolytes.

2.3. Characterization

The rheological behavior of the suspensions and binder solutions was measured with a rotational viscosimeter (Physica MCR 100, Anton Paar Germany GmbH, Ostfildern, Germany) at shear rates between 10 and 1000 s^{-1} by an increasing (up) shear rate sweep with a logarithmic decrease of measurement point duration (9.3 s to 3.9 s), a dwelling time of 60 s at 1000 s^{-1}, and a decreasing (down) shear rate sweep with a logarithmic increase of measurement point duration. The microstructures of the sintered layers were investigated by scanning electron microscope analyses of sample cross-sections and surfaces (Zeiss Gemini Ultra 55, Carl Zeiss NTS GmbH, Oberkochen, Germany, and Phenom, Fei Europe, Eindhoven, Netherlands). The gas tightness of the electrolyte layers was determined by a helium leak test (HLT260, Pfeiffer Vacuum GmbH, Asslar, Germany). The helium flow through the 50 mm × 50 mm half-cells was determined with a mass spectrometer at a pressure difference of approx. 1000 hPa. The values were normalized to the measured area (16 cm^2) and to a pressure difference of 100 hPa, which is similar to the pressure conditions in a stack. The deflection after the sintering process was measured using laser topography (CT200, Cyber Technologies GmbH, Ingolstadt, Germany).

The electrochemical characterization of single cells with an active cell area of 16 cm^2 was performed with 1000 standard cm^3 min^{-1} (sccm) 97% H_2 + 3% H_2O as fuel gas and 1000 sccm air as oxidant at temperatures from 650 to 900 °C [26]. In order to obtain more detailed information about the electrochemical performance of the cell functional layers, electrochemical impedance spectroscopy (EIS) was carried out on the single cells with an active cathode area of 10 mm × 10 mm and two auxiliary electrodes in the gas flow direction in front of and behind the cathode, while the total anodic ($H_2 + H_2O$) and cathodic ($O_2 + N_2$) gas flow rates were each maintained at a constant value of 250 sccm. The data were obtained by a Solartron-1260 frequency response analyzer (Solartron Analytical AMETEK Advanced Measurement Technology GmbH, Meerbusch, Germany) under open-circuit conditions in a frequency range from 0.1 Hz to 1 MHz at temperatures from 550 to 900 °C using a fuel gas humidity of 60–63% and cathodic partial pressures (p_{O_2}) from 0.02 to 1 atm. The high water content was used to reduce the anodic polarisation losses to a minimum thereby making the deconvolution of the cathodic contributions simpler. From the recorded impedance data, the corresponding distribution function of relaxation times (DRTs) was calculated and used to fit the characteristic parameters of an equivalent circuit model by the complex nonlinear least-squares (CNLS) approximation method [21].

3. Results and discussion

3.1. Suspensions and coating process

The rheological behavior of the anode and electrolyte roll coating suspensions is shown in Fig. 2 and is compared to the viscosity of

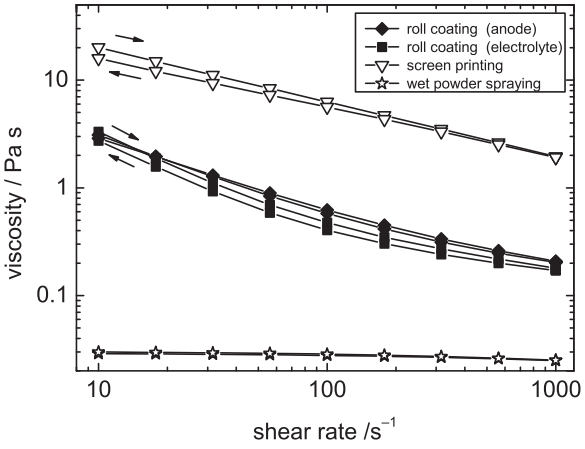

Fig. 2. Dynamic viscosity of anode and electrolyte roll coating suspensions as a function of increasing and decreasing shear rate sweep, in comparison with suspensions established for other wet chemical coating technologies. The screen printing paste shown was based on terpineol and ethyl cellulose [10]. The wet powder spraying suspension was prepared from TZ-8Y as received and DBE/ethyl cellulose [22].

suspensions used for other well-established wet chemical coating technologies. As the viscosities of the increasing shear rate sweep are very close to those of the down sweep the measurement was not significantly affected by a potential thixotropy of the samples. The viscosity curve of the roll coating suspension lies between the viscosities of screen-printing pastes and the suspensions for wet powder spraying. The roll coating suspensions display a sheer-thinning behavior with a viscosity around 0.2 Pa s at high shear rates around 1000 s^{-1}. Such shear rates and higher are expected to occur during the coating process in the suspension between the substrate and the applicator roll. The shear-thinning behavior is especially desirable for roll coating on pre-sintered, porous supports. The low viscosity of the sheared suspension enhances the transport from the applicator roll to the substrates and the homogeneous spreading on the substrate's surface, while the increase in viscosity after coating prevents full infiltration into a porous support and improves the handling of the samples as the coating keeps its shape. Such shear-thinning suspensions are easier to process with reverse roll coating than with forward roll coating, as the lower pressure gradient of the suspension in the downstream meniscus between applicator roll and substrate restrains ribbing effects [14,19]. It was somewhat surprising that the quite brittle and sometimes slightly bent pre-sintered substrates did not break during the coating process. The fact that only a linear load occurs between the rubber-coated transport and applicator roll enables the coating of these substrates without failure. This is regarded as an advantage compared to the established screen printing process, where the sample is faced with a more inhomogeneous load distribution during coating and similar substrates break easily at their edges. The soft green tapes could also be coated without problems, the sample transport worked flawlessly and the samples did not show any significant deformation. Although no stacks were assembled in this work, relatively large substrates were used for the coating process in order to show the scalability of the roll coating process. Furthermore, it should be noted that the first 5–10 mm of the feeding side of the samples were not evenly coated. This edge effect will dominate more the smaller the samples become and will be eliminated if continuous green tapes are coated.

3.2. Deflection

In order to assemble and contact the cells for operation, they must be sufficiently flat. As the anode substrates consists of larger grains and pores than the electrolyte, the substrate further shrinks even after the electrolyte is already densified [10,27]. As the electrolyte is on the top, this sintering mismatch leads to a convex bending of the multilayer compound, which was also observed for the roll-coated cells (Fig. 3). The bending in general and the occurrence of edge effects in particular strongly depended on whether the air or foil side of the tape-cast substrate was coated; the total deflection measured 2.1 and 2.6 mm for the coatings on the air and foil side, respectively. This was caused by an inherent inhomogeneity in the microstructure of the tape-cast supports, as the segregation behavior of the solvent and binder during the drying process results in larger pores on the foil side [23]. This in turn leads to a larger shrinkage of the foil side in comparison to the air side of the tape-cast support and therefore to an inherent bending towards the foil side, which superposes the sintering mismatch effect of the multi-layers. Depending on the coating side of the tape (air or foil side), the deflections are aligned in the same direction (Fig. 3a) or opposite to each other (Fig. 3b). In the latter case, the effect is very pronounced as the edges bend in a different direction than towards the center of the sample. This is further superimposed by the torques exerted by the sample's own weight. Whereas convex deflections are affected relatively uniformly, the torques caused by gravity almost diminish on the edges of concavely bended samples, yielding larger shape inhomogeneities [10]. This was found for the coatings on the foil side (Fig. 3b) and is more likely to affect later processing, for example, screen-printing the cathode. Therefore, all subsequent coatings were applied on the air side. To reduce the deflection below 1 mm, the half-cells were flattened by applying a load in a specially designed furnace at a temperature of 50 K below the sintering temperature. These larger half-cells were cut into dimensions of 50 mm × 50 mm for electrochemical characterization, resulting in a deflection below 150 μm.

3.3. Microstructural characterization

As seen from the cross-sections in Fig. 4(a) and (b) and the top view in Fig. 5, the electrolyte layer is well densified and exhibits

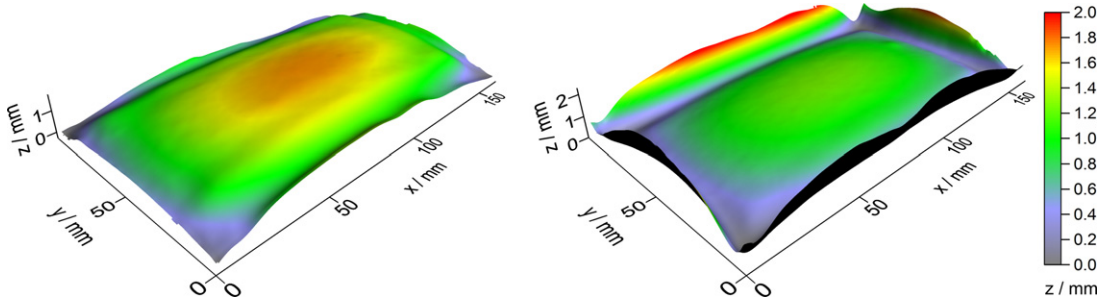

Fig. 3. Laser topographic images of coated green tape-cast anode substrates after sintering, shown on the coated side: (a) with anode and electrolyte on the air side of the tape-cast substrate, total deflection 2.1 mm, (b) coated on the foil side, total deflection 2.6 mm. Vertical exaggeration: 10 times.

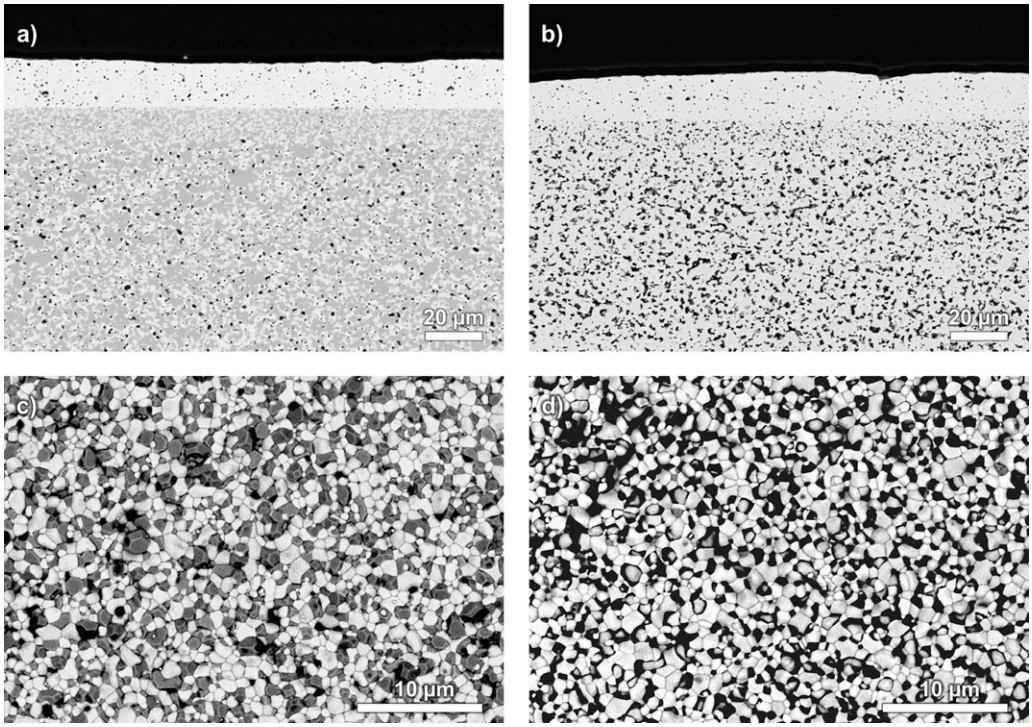

Fig. 4. SEM images of a roll-coated half-cell for which the anode and electrolyte were applied on the air side of green tape-cast substrates (a) cross-section of sintered half-cell in the oxidized state, (b) cross-section after reduction, (c) top view of the sintered anode layer, white: zirconia, gray: nickel oxide and (d) anode after reduction, white: zirconia, gray: nickel, black: pores.

only closed residual pores after sintering. Its thickness was found to be 17–18 and 14–16 μm for the coatings on the green and pre-sintered tapes, respectively (Table 2). This is larger than for typical screen-printed electrolyte layers, which typically show a thickness of around 7 μm [10,28]. In the ongoing work, we aim to reduce the layer thickness by adjusting the coating parameters. The ratio of the rotation speed of the dip, applicator and transport roll, in particular, strongly influence the thickness of the resulting layer. However, at the same time, the suspension has to be optimized to form a thin uniform film without ribbing on the rolls and the substrate, as in a thinner layer the leveling of the liquid films on the rolls and on the substrate is strongly hindered [29]. According to the theory of Orchard, half of the thickness hinders leveling by a factor of eight [30]. The anode exhibits a thickness of 11–13 and 8–10 μm for the coatings on green and pre-sintered substrates, respectively. The latter is comparable to screen-printed or slip-cast layers in Jülich standard cells with a thickness of approx. 7 μm [28]. Even though the anode is almost dense in the oxidized state (Fig. 4a and c), a clearly enhanced micro-porosity of this layer was found after reduction (Fig. 4b and d). Therefore, this results in sufficient gas permeation through the anode, which is a prerequisite for the electrochemical characterization given below.

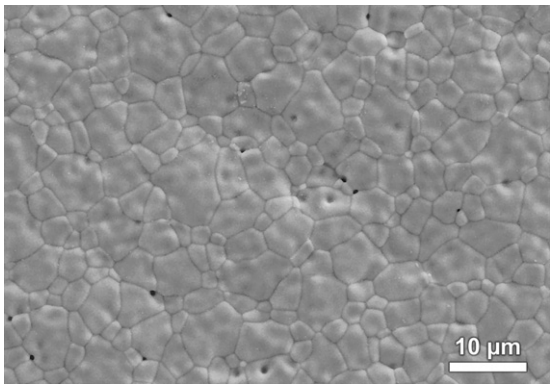

Fig. 5. SEM top view of the as-sintered electrolyte of a roll-coated half-cell for which the anode and electrolyte were applied on the air side of a green tape-cast substrate.

3.4. Leak rates

The good gas tightness of the electrolyte layers indicated by the microstructure was verified by a He permeability test. The average leak rates obtained in the oxidized state for the cells used later in the electrochemical characterization are given in Table 2. All values of the cells with an anode were approx. one order of magnitude lower than the maximum tolerated for the Jülich standard cell, which is 2.0×10^{-5} hPa dm^3 s^{-1} cm^{-2}. As the anode displays a finer microstructure than the substrate, the leak rate increases when the anode is omitted. As the cells required the cathode to be sintered in air and were subjected to an electrochemical characterization, no leak rates were taken in the reduced states. As known from Jülich standard cells, the anode already appears to be dense in the oxidized state (Fig. 4c). Typical leak rates of sintered samples without an electrolyte are higher than for those with an electrolyte, but the values can lie in a similar range. Therefore, the leak rates were also determined in the reduced state for a second series and compared with Jülich standard cell prepared by screen printing (Fig. 6). Since screen printing was only used for pre-sintered supports, pre-sintered substrates were used for both groups. Again, all leak rates for the oxidized state were significantly lower than the quality control threshold. The leak rates increased significantly during the reduction, but the values were in the same range already known from Jülich standard cells (Fig. 6). It can be concluded that similar leak rates to those for standard cells can be achieved by roll-coated half-cells. However, the adaptation of the roll-coated layer thicknesses is a remaining task.

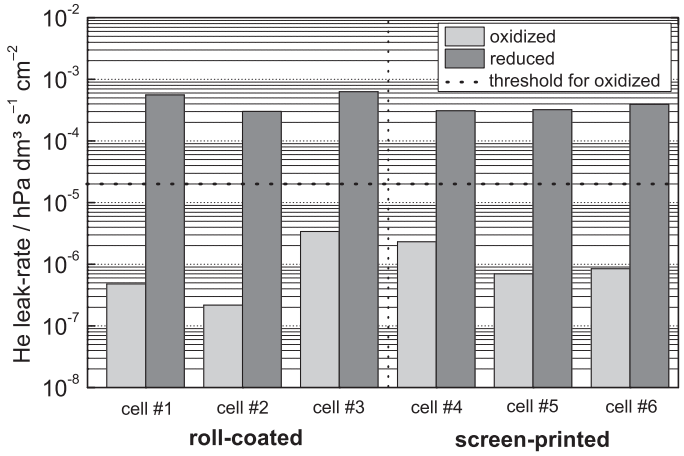

Fig. 6. He leak rates of the roll-coated half-cells in comparison with screen-printed Jülich standard cells in the oxidized and reduced state. The functional layers of half-cells were coated on the air side of the tape-cast supports.

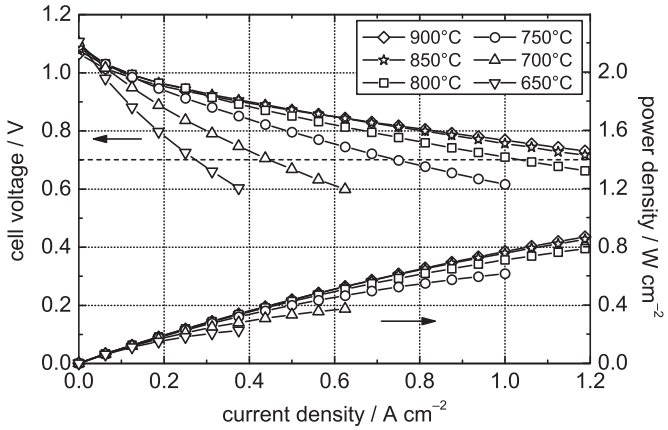

Fig. 7. Current–voltage and current–power curves of a cell with roll-coated anode and electrolyte (coated on green tape) with an active area of 16 cm² as a function of the temperature (cell #7 in Table 3).

3.5. Electrochemical performance

The open-circuit voltages and current densities were measured for two similar cells of both manufacturing variants (coatings on green and pre-sintered supports) between 650 and 850 °C (Table 3). Cell #7, with the roll-coated layers applied on green tapes, yielded a similar open-circuit voltage as the Jülich standard LSM cells. However, the second similarly prepared cell and the two cells prepared from pre-sintered substrates display slightly lower open-circuit voltages. The current–voltage (i–V) and current–power (i–p) curves of single cells are shown in Figs. 7 and 8. At 800 °C and 0.7 V, the cells with roll-coated anodes and electrolytes and screen-printed LSM cathodes yielded an average current density of around 1.0 A cm^{-2}, which corresponds to a power density of 0.7 W cm^{-2}. The performance was lower than the performance of screen-printed Jülich standard cells with an LSM cathode, which yield a current density of 1.49 ± 0.08 A cm^{-2} at 800 °C, 0.7 V (Table 3 and [31]).

This was further analyzed by electrochemical impedance spectroscopy of cells with an active area of 1 cm². The roll-coated samples exhibited a higher ohmic resistance R_0 than standard cells, as was already observed in the raw impedance data in Fig. 9, as the real part of the impedance is larger at high frequencies. The distribution of relaxation times (DRT) was calculated from the impedance data (Fig. 10) and then the parameters of an equivalent circuit were obtained by CNLS fitting the DRT data (Fig. 11)

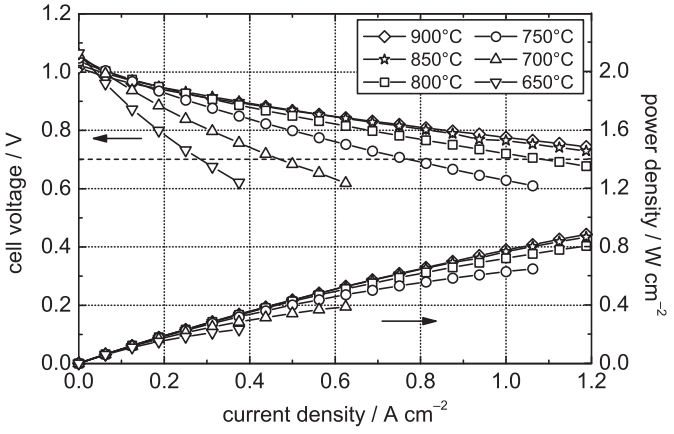

Fig. 8. Current–voltage and current–power curves of a cell with roll-coated anode and electrolyte (coated on pre-sintered substrate) with an active area of 16 cm² as a function of the temperature (cell #9 in Table 3).

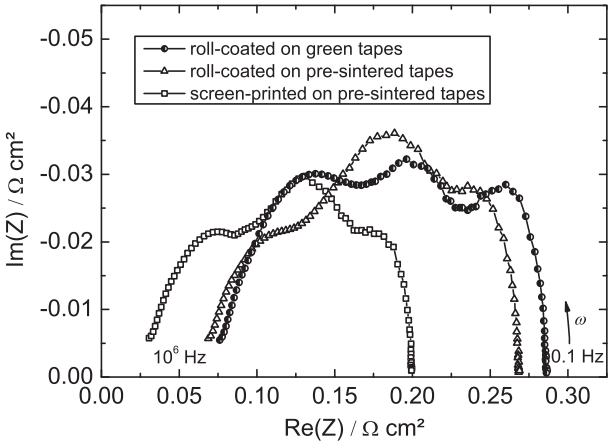

Fig. 9. Nyquist plots of electrochemical impedance spectroscopy of cells (with an anode) of the two roll-coated cell variants and a Jülich standard screen-printed cell with an active cell area of 1 cm² measured at 800 °C in H_2 (60% H_2O) and air under open-circuit conditions. For better readability, the axes are scaled different.

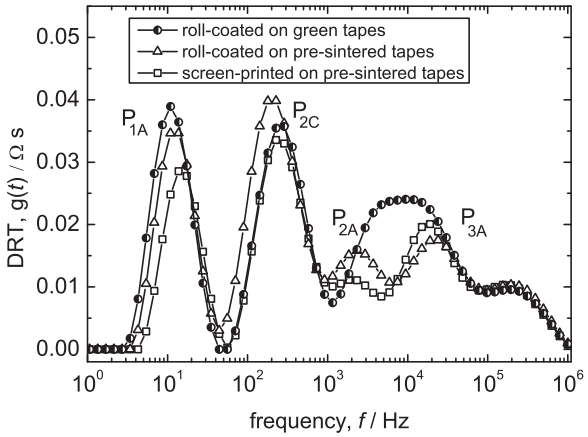

Fig. 10. DRTs of the different cells (with an anode) at 800 °C of the two roll-coated cell variants and a Jülich standard screen-printed cell.

[21]. Fig. 11 includes an additional cell without an anode for further interpretation of the data. However, for the sake of clarity this cell was omitted in the graphs of Figs. 9 and 10. The ohmic resistance R_0 and the polarization losses were obtained; the latter are represented by the processes P_{1C}, P_{2A}, and P_{3A} which were modeled by a

Table 3
OCVs and current densities of roll-coated single cells and Jülich standard cells with an LSM cathode at varying temperatures (active area of 16 cm^2 in H_2).

Temperature (°C)	Coating on green tapes				Coating on pre-sintered tapes				Standard LSM cells[a]	
	UOVC (mV)		j at 0.7 V (A cm^{-2})		U_{OVC} (mV)		j at 0.7 V (A cm^{-2})		U_{OVC} (mV)	j at 0.7 V (A cm^{-2})
	Cell #7	#8	#7	#8	#9	#10	#9	#10		
650	1107	1073	0.27	0.27	1065	1076	0.27	0.27	1104 ± 7	0.35 ± 0.03
700	1103	1066	0.46	0.44	1059	1070	0.47	0.45	1097 ± 5	0.63 ± 0.04
750	1094	1054	0.74	0.70	1048	1060	0.75	0.72	1092 ± 6	1.03 ± 0.06
800	1086	1042	1.04	0.93	1037	1050	1.07	1.02	1081 ± 5	1.49 ± 0.08
850	1076	1034	1.26	1.10	1025	1039	1.33	1.25	1072 ± 5	1.88 ± 0.10
900	1065	1015	1.34	1.09	1015	1031	1.44	1.33	1062 ± 4	2.13 ± 0.14

[a] The quantities for the Jülich standard cells (slip-cast or screen-printed anodes and electrolytes) are average values for 6 × 2 cells.

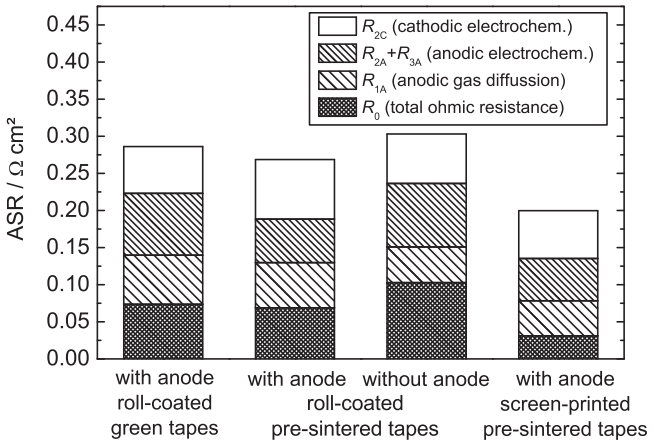

Fig. 11. Calculated components of the area-specific resistance of three roll-coated cell variants and a Jülich standard screen-printed cell at 800 °C in H_2 (60% H_2O) and air obtained by CNLS fitting the DRTs. R_0 denotes the total ohmic resistance, R_{1A}, $R_{2A}+R_{3A}$ denote the anodic and R_{2C} the cathodic polarization resistances (as described in the text).

RQ element (formed by a resistor, *R*, and a constant phase element, *Q*, in parallel) and P_{1A} and P_{2C} which were modeled by a generalized Warburg element of finite length (G-FWS) and a Gerischer element, respectively. In previous work [21], by varying the partial pressure of the cathode, it could be shown that P_{1A} can be attributed to the resistance of the gas diffusion in the anode support, P_{2A} and P_{3A} correspond to electrochemical reactions in the anode layer (i.e. gas diffusion coupled with charge transfer reaction and ionic transport), whereas P_{2C} describes electrochemical polarization of the cathode side [32,33]. The corresponding area specific polarization resistances to those processes were denoted R_{1A}, $R_{2A}+R_{2A}$, and R_{2C}, respectively.

The ohmic resistance of cells with roll-coated anodes and electrolytes was found to more than twice as high as the ohmic resistance of the screen-printed Jülich standard cell (0.073 and 0.069 Ω cm^2 vs. 0.031 Ω cm^2 at 800 °C, Fig. 11) which reflects the fact that the roll-coated electrolyte was more than twice as thick than the screen-printed ones. For the same cells, the comparison of the anodic part R_{1A} of the total ASR is higher for the thicker roll-coated anodes (0.066 and 0.061 Ω cm^2 for the roll-coated cells vs. 0.047 Ω cm^2 for the screen-printed cell). Previous works showed that the polarization resistance R_{1A} caused by the gas diffusion transport in the substrates was independent of the anode layer [21,33]. Nevertheless, the substrates of the cells tested in the past were manufactured by warm-pressing which resulted in a rather difficult to reproduce microstructure and therefore also to a large scattering of R_{1A} [33]. However, in this study unexpectedly R_{1A} appears to be also influenced by the anode layer. This fact may be explained by the fact of an additional gas diffusion polarization contribution originating from the anode layer having a similar characteristic frequency than process P_{1A}. Even thought this circumstance needs to be examined more precisely in future studies, in this study it can be concluded that the permeation of the fuel is lower for the thicker roll-coated anodes and yielded to a higher value of R_{1A}. This was confirmed by testing a cell with a roll-coated electrolyte of the same thickness as the other roll-coated samples but without an anode (third column in Fig. 11). The resistance R_{1A} of this cell was found to be 0.047 Ω cm^2 which is the same as for the standard cell with the thinner screen-printed anode. Obviously, this remaining resistance is due to the anode substrate itself. This agrees with a recent investigation confirming that a range of the thicknesses exists for the anode layer, which prevents the cell performance being affected by the gas diffusion inside the anode [28]. Unless the thickness of the slip-cast anode exceeded 13 μm, the cell performance remained constant when operated on relatively dry 97% H_2 + 3%H_2O as the fuel. As the EIS data in the present work were obtained at a much higher humidity (60–63%), it can be concluded that this critical thickness decreases. This effect was already observed in the roll-coated anodes within a thickness range from 8 to 13 μm. The cell without an anode shows a significantly increased ohmic resistance R_0 which indicates that the contact resistance between the electrolyte and substrate is higher than between electrolyte and anode layer. This is due to the fact that the contact area of the 8YSZ phase is larger for the finer and denser microstructure of the anode layer. As expected, the anodic electrochemical contribution $R_{2A}+R_{3A}$ of the ASR is worst for the cell without any anode layer (0.086 Ω cm^2) since there are less triple-phase boundaries in the coarser anode substrate compared to the anode layer. It is interesting to note that the roll-coated anodes applied on green tapes also show a large $R_{2A}+R_{3A}$ (0.084 Ω cm^2) whereas the roll-coated anodes on applied pre-sintered supports behave similarly to the screen-printed standard cells (0.059 Ω cm^2 vs. 0.057 Ω cm^2). An explanation for this phenomenon could be that the pre-sintered cells shrink 10.5% during the final sintering step, whereas the green tapes shrink 17.6% [23], exerting larger compressive forces on the coating during the heat treatment. This enhances not only the sintering density but also the grain growth [34] which in turn will decrease the amount of triple-phase boundaries. However, further microstructural investigations are necessary to confirm this assumption. The cathodic resistance R_{2C} is constant for all cells except for the value of the roll-coated cell with an anode on a pre-sintered support, which is unexpectedly higher. The reason for this result is still unclear.

Considering the observed facts, the roll coating process is being improved in order to reduce the layer thickness. The spreading behavior of the suspension, i.e. surface and interface energies, has yet to be investigated. Nevertheless, our results are promising with respect to industrial-scale production, where the cost reduction potential is always the main driving force for the introduction of new manufacturing technologies.

4. Conclusions

Anode-supported solid oxide fuel half-cells were successfully produced by a combination of tape casting of the substrate and roll coating of the functional layers anode and electrolyte. The roll coating process represents a new manufacturing technology for functional ceramic layers and was successfully applied to SOFCs. Furthermore, it was demonstrated that the substrate, anode and electrolyte could be sintered in one step at 1400 °C for 5 h. After screen printing an LSM cathode followed by a second thermal treatment at 1100 °C for 3 h, the cell was electrochemically characterized. Open-circuit voltages better than 1.0 V indicated sufficient gas tightness for the roll-coated electrolyte. At 800 °C and 0.7 V, a current density of approx. 1.0 A cm^{-2} with a corresponding power density of 0.7 W cm^{-2} was achieved. To increase the electrochemical performance especially the thickness of the applied layers should be decreased by adjusting suspension and coating parameters. Our results demonstrate that the fabrication of SOFCs by tape casting, roll coating and co-firing is a new cost-effective and feasible manufacturing route for planar SOFCs. Together with the results achieved with a laboratory machine in this paper, there is a large potential for using this method for the mass production of solid oxide fuel cells.

Acknowledgments

The authors sincerely thank V.A.C. Haanappel and his team (IEK-3) for performing the electrochemical characterization, D. Sebold (IEK-1) for SEM analysis, N.H. Menzler (IEK-1) for his valuable support and discussions, and W. Schafbauer (IEK-1) for the preparation of the anode substrates. Mrs. J. Carter-Sigglow has contributed to this work by her careful revision of the English usage.

Appendix A. Supplementary data

Supplementary data associated with this article can be found, in the online version, at doi:10.1016/j.jpowsour.2011.07.063.

References

[1] S. Linderoth, P.H. Larsen, M. Mogensen, P.V. Hendriksen, N. Christiansen, H. Holm-Larsen, Mater. Sci. Forum 539–543 (2007) 1309.
[2] N. Christiansen, J.B. Hansen, H. Holm-Larsen, S. Linderoth, P.H. Larsen, P.V. Hendriksen, A. Hagen, ECS Trans. 7 (2007) 31.
[3] T. Horita, H. Kishimoto, K. Yamaji, M.E. Brito, Y. Xiong, H. Yokokawa, Y. Hori, I. Miyachi, J. Power Sources 193 (2009) 194.
[4] L.G.J. de Haart, J. Mougin, O. Posdziech, J. Kiviaho, N.H. Menzler, Fuel Cells 9 (2009) 794.
[5] R. Steinberger-Wilckens, H.P. Buchkremer, J. Malzbender, L. Blum, L.G.J. de Haart, M. Pap, in: P. Connor (Ed.), Proc. 9th European Solid Oxide Fuel Cell Forum, Switzerland, 2010, pp. 2–31.
[6] F. Han, A. Leonide, T. van Gestel, H.P. Buchkremer, in: P. Connor (Ed.), Proc. 9th European Solid Oxide Fuel Cell Forum, Switzerland (2010), 11-1.
[7] W. Schafbauer, R. Kauert, N.H. Menzler, H.P. Buchkremer, in: R. Steinberger-Wilckens, U. Bossel (Eds.), Proc. 8th European Solid Oxide Fuel Cell Forum, Oberrohrdorf, Switzerland, 2008, B0512.
[8] P. Von Dollen, S. Barnett, J. Am. Ceram. Soc. 88 (2005) 3361.
[9] J.W. Phair, J. Am. Ceram. Soc. 91 (2008) 2130.
[10] R. Mücke, N.H. Menzler, H.P. Buchkremer, D. Stöver, J. Am. Ceram. Soc. 92 (2009) S95.
[11] C. Wang, W.L. Worrell, S. Park, J.M. Vohs, R.J. Gorteb, J. Electrochem. Soc. 148 (2001) A864.
[12] N. Minh, A. Anumakonda, B. Chung, R. Dhoshi, J. Ferall, J. Guan, G. Lear, Electrochem. Soc. Proc. 99-19, 1999, p. 68.
[13] H. Benkreira, R. Patel, Chem. Eng. Sci. 48 (1993) 2329.
[14] D.J. Coyle, in: E.D. Cohen, E.B. Gutoff (Eds.), Modern Coating and Drying Technology, Wiley-VCH, New York, 1992, pp. 63–116.
[15] K. Noda, M. Yamagami, M. Yamamoto, H. Sato, H. Itaya, A. Okajima, M. Yamada, Jpn. J. Appl. Phys. 42 (2003) 5722.
[16] V. Metha, J. Smith Cooper, J. Power Sources 114 (2003) 32.
[17] C. Münch, Process and Apparatus for Applying Solutions, U.S. pat. 1,847,065 (1932).
[18] G. Broughton, L.W. Egan, R. Sturken, TAPPI 33 (1950) 314.
[19] J. Greener, S. Middleman, Ind. Eng. Chem. Fundam. 20 (1981) 63.
[20] S.K. Han, D.M. Shin, H.Y. Park, H.W. Jung, J.C. Hyun, Eur. Phys. J. Spec. Topics 166 (2009) 107.
[21] A. Leonide, V. Sonn, A. Weber, E. Ivers-Tiffée, J. Electrochem. Soc. 155 (2008) B36.
[22] K. Brands, Entwicklung und Charakterisierung eines metallischen Substrats für nanostrukturierte keramische Gastrennmembranen, PhD Thesis, Energy & Environment 72, Forschungszentrum Jülich Zentralbibliothek, Verlag, 2010.
[23] W. Schafbauer, Entwicklung und Herstellung von foliengegossenen, anodengestützten Festoxidbrennstoffzellen, PhD Thesis, Energy & Environment 66, Forschungszentrum Jülich Zentralbibliothek, Verlag, 2010.
[24] N.H. Menzler, M. Zahid, H.P. Buchkremer, in: J. Kriegesmann (Ed.), Technische Keramische Werkstoffe, Deutscher Wirtschaftsdienst, Höhr-Grenzhausen, 2004, pp. 1–21 (chapter 3.4.6.1).
[25] A. Gubner, T. Nguyen-Xuan, J. Remmel, M. Bram, L.G.J. (Bert) de Haart, in: U. Bossel (Ed.), Proc. of 7th Eur. Solid Oxide Fuel Cell Forum, Oberrohrdorf, 2006, B042.
[26] V.A.C. Haanappel, M. Smith, J. Power Sources 171 (2007) 169.
[27] J. Kanters, U. Eisele, J. Rödel, J. Am. Ceram. Soc. 84 (2001) 2757.
[28] N.H. Menzler, V.A.C. Haanappel, J. Power Sources 195 (2010) 5340.
[29] T. Matsuda, W.H. Brendley Jr, J. Coat. Technol. 51 (1979) 46.
[30] S.E. Orchard, Appl. Sci. Res. 11A (1962) 451.
[31] V.A.C. Haanappel, N. Jordan, A. Mai, J. Mertens, J.M. Serra, F. Tietz, S. Uhlenbruck, I.C. Vinke, M.J. Smith, L.G.J. de Haart, J. Fuel Cell Sci. Technol. 6 (2009) 021302–21311.
[32] V. Sonn, A. Leonide, E. Ivers-Tiffée, J. Electrochem. Soc. 155 (2008) B675.
[33] A. Leonide, S. Ngo Dinh, A. Weber, E. Ivers-Tiffée, in: R. Steinberger-Wilckens, U. Bossel (Eds.), Proc. of 8th Eur. Solid Oxide Fuel Cell Forum, Oberrohrdorf, 2008, p. A0501.
[34] D.J. Green, O. Guillon, J. Rödel, J. Eur. Ceram. Soc. 28 (2008) 1451.